Soft Matter

Cite this: *Soft Matter*, 2012, **8**, 9073

www.rsc.org/softmatter

PAPER

Highly ordered superstructures of single wall carbon nanotube–liposome complexes†

Tae-Hwan Kim,‡ Changwoo Do,§ Shin-Hyun Kang, Min-Jae Lee, Sung-Hwan Lim and Sung-Min Choi*

Received 10th April 2012, Accepted 28th June 2012
DOI: 10.1039/c2sm25827g

A general and easy way to fabricate highly ordered single wall carbon nanotube (SWNT) superstructures with complex architectures is essential for various practical applications of SWNTs. Here, we report for the first time the highly ordered self-assembled superstructures of negatively charged SWNTs and cationic liposome complexes, which exhibit two kinds of superlattices of SWNTs, a centered rectangular superlattice of SWNTs intercalated in a multilamellar structure, and an inverted centered rectangular columnar packing with SWNTs at the centers of columns, depending on the spontaneous curvature and surface charge density of the lipid monolayer. The results of this study can provide a new route to fabricate highly ordered superlattices of SWNTs with new or enhanced functionalities, utilizing biomolecular self-assembling behavior.

Introduction

Single wall carbon nanotubes (SWNTs) are one of the most important materials in the field of nanotechnologies[1–5] due to their remarkable electrical, thermal and mechanical properties[6–8] and provide a broad spectrum of potential applications. Recently, the unique properties of SWNTs have generated great interest because of their biological or biomedical applications as well.[9–16] Despite the extraordinary properties of SWNTs, however, there are still many issues remaining to be resolved for practical applications. One of the key issues is how to fabricate highly controlled and ordered assembly of SWNTs with well-defined morphology, regularity, and direction, which will collectively enhance the physical properties of SWNTs. A great deal of effort has been made to develop new routes to assemble SWNTs into novel superstructures using methods such as solvent evaporation,[17] patterning substrates,[18] mechanical stretching,[19] shear flow,[20] and applying an electrical field.[21] The majority of assembled SWNT superstructures achieved so far, however, have been limited to simple ones such as preferentially oriented SWNTs on substrates or nematic SWNTs in bulk. Recently, a new effort has been made to utilize the phase behavior of a block copolymer system as a route to fabricate multi-dimensional SWNT superstructures.[22] However, general and easy ways of fabricating highly ordered SWNT superstructures with complex architectures have not been fully exploited yet.

In biological systems, a large variety of complex structures are formed through cooperative self-assembly of various constituting biomolecules and components. Inspired by the novel self-assembling behaviors in biological systems, fabrications of many new nanostructured materials have been successfully demonstrated. Recently, the DNA–lipid complex systems have been extensively investigated, showing that they exhibit various ordered superstructures such as intercalated lamellar or hexagonal structures through electrostatic interactions.[23–27] Self-assembling behavior of nanoparticles is highly dependent on their dimensionality. Considering the one-dimensional nature of DNA, the rich self-assembling behavior of a DNA–lipid complex is highly inspiring in the search for a new route for highly ordered superstructures of SWNTs which also have one-dimensional nature. Recently, SWNTs have attracted intensive attention as possible vehicles for drug delivery.[28–35] Therefore, understanding the interactions of SWNTs with lipid bilayers is of great interest for biological or biomedical applications of SWNTs.

In this article, we report the highly ordered superstructures of negatively charged SWNTs and cationic liposome (CL) complexes, which exhibit two kinds of centered rectangular columnar phases: an intercalated lamellar structure with a centered rectangular columnar superlattice of SWNTs and an inverted centered rectangular columnar packing with SWNTs at the centers of columns. Here, the structures were controlled by varying the spontaneous curvature and the surface charge density of the lipid monolayer. To the best of our knowledge, this

Department of Nuclear and Quantum Engineering, KAIST, 291 Daehak-ro, Yuseong-gu, Daejeon, 305-701, Republic of Korea. E-mail: sungmin@kaist.ac.kr

† Electronic supplementary information (ESI) available: Detailed preparation of p-SWNT25, ^{1}H-NMR and UV-vis-NIR measurements of p-SWNT25, DLS and zeta potential measurements of p-SWNT25–CL complexes, and AFM measurements of p-SWNT25. See DOI: 10.1039/c2sm25827g

‡ Current address: Neutron Science Division, Department of Reactor Utilization and Development, Korea Atomic Energy Research Institute, 1045 Daedeok-daero, Yuseong-gu, Daejeon, 305-353, Republic of Korea.

§ Current address: Biology and Soft Matter Division, Neutron Sciences Directorate, Oak Ridge National Laboratory, Oak Ridge, TN 37831, USA.

is the first demonstration of two-dimensional centered rectangular arrays of SWNTs using molecular self-assembly.

Experimental

Materials

Dioleoyltrimethylammoniumpropane (DOTAP) and dioleoylphosphatidylethanolamine (DOPE) were purchased from Avanti Polar Lipids. Cetyltrimethylammonium hydroxide (CTAOH) and 4-vinylbenzoic acid (VBA) were purchased from Aldrich. Sodium 4-styrenesulfonate (NaSS) was purchased from Fluka. Purified HiPco single wall carbon nanotubes (purity: >90 wt%) were purchased from Carbon Nanotechnologies Inc. A water-soluble free-radical initiator, VA-044 (2,2′-azobis[2-(2-imidazolin-2-yl)propane] dihydrochloride), was purchased from Wako Chemicals. D_2O (99.9% by mole deuterium enriched) was purchased from Cambridge Isotope Laboratory. H_2O was purified using a Millipore Direct Q system immediately before use. Cetyltrimethylammonium 4-vinylbenzoate (CTVB) was synthesized through neutralization of VBA in the presence of a slight stoichiometric excess of CTAOH followed by repeated crystallization. Further details of the procedure are described elsewhere.[36]

SAXS measurements

SAXS measurements were performed on the 4C1 beamline at the Pohang Accelerator Laboratory (PAL), Republic of Korea, where a W/B4C double multilayer monochromator delivered monochromatic X-rays with a wavelength of 0.1608 nm and wavelength spread $\Delta\lambda/\lambda = 0.01$. A 2-dimensional CCD camera (Mar CCD, Mar USA, Inc. CCD165) was used to collect the scattered X-rays. Sample cells with a thickness of 0.8 mm were used with a mica window and sealed with epoxy. The sample to detector distance (SDD) was 1 m, covering the q range of 0.3 $nm^{-1} < q < 3.6\ nm^{-1}$, where $q = (4\pi/\lambda)\sin(\theta/2)$ is the magnitude of the scattering vector and θ is the scattering angle. The q range was calibrated using SEBS (polystyrene-*block*-poly(ethylene-*ran*-butylene)-*block*-polystyrene). All measurements were performed at 25 °C.

Zeta potential measurements

Zeta potential measurements were carried out using a ZetaPlus zeta potential analyzer (Brookhaven Instruments Corporation). The zeta potential was calculated using Smoluchowski's equation *via* the measurement of the eletrophoretic mobility.

DLS measurements

DLS measurements were carried out using a ZetaPlus particle size analyzer ($\lambda = 659$ nm, scattering angle = 90°, Brookhaven Instruments Corporation).

UV-vis-NIR measurements

UV-vis-NIR measurements were carried out using a Lambda 750 (Perkin-Elmer Corporation) model spectrometer and 2 mm path length quartz cells in D_2O at room temperature.

Atomic force microscopy (AFM) measurements

The AFM images were taken in tapping mode by using a VEECO AFM instrument (Nanoman, SECPM). A p-SWNT25 dispersion was spin-coated on silicon wafers (at 4000 rpm for 1.5 min). To prepare samples of bare SWNTs, p-SWNT25 deposited on silicon wafers was burned for 4 h at 330 °C to remove the CTVB/NaSS layer absorbed on the SWNTs.

Results and discussion

The negatively charged and individually isolated functionalized SWNTs (p-SWNT25) were prepared by dispersing SWNTs (2 mg mL^{-1}) in water using a cationic surfactant, cetyltrimethylammonium 4-vinylbenzoate (CTVB, 5 mg mL^{-1}), which has polymerizable counterions (VB^-), and an anionic hydrotropic salt, sodium styrenesulfonate (NaSS, 25 mol% relative to CTVB concentration), which induces a negative surface charge of p-SWNT25.[36] The surfactant monolayer on the SWNT was permanently fixed through *in situ* free radical copolymerization of the counterions (VB^- and SS^-)[36,37] (ESI†), followed by ultracentrifugation (*ca.* 110 000*g*) and freeze drying[37,38] (ESI†). The UV-vis-NIR spectra of the p-SWNT25 dispersion in water showed a sharp van Hove transition, which is typical for individually isolated SWNT in solution[39–44] (ESI†). The p-SWNT25 was very stable and highly re-dispersible in water by only a few minutes of mild vortex mixing, even after harsh processing such as freeze drying. Considering that the structure (diameter) of the polymerized CTVB particle is not changed by adding the NaSS,[36] the structure of p-SWNT25 is expected to be essentially the same as that of p-SWNT (functionalized SWNTs fabricated in exactly the same procedure as p-SWNT25, except that NaSS was not added[37,38]); isolated SWNTs of an average diameter of 1.0 nm are cylindrically encapsulated by polymerized surfactant monolayers with a thickness of about 2.0 nm, resulting in a diameter of 5.0 nm for the p-SWNT25 (Fig. 1). The length of p-SWNT25 is also similar to that of p-SWNT (*ca.* 500 nm). These were confirmed by AFM measurements of p-SWNT25 (ESI†). The negative surface charge density of p-SWNT25 was confirmed by zeta potential measurement, resulting in -32.2 ± 2.2 mV (ref. 45).

For a systematic control of interactions between SWNT and lipids, which may allow the various phase behaviors of SWNTs in a lipid matrix, a mixed CL system with different spontaneous curvatures and surface charge densities of lipid

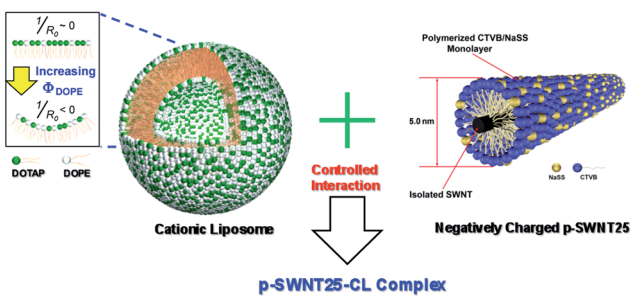

Fig. 1 A schematic view of the interaction control between the p-SWNT25 and CL. For the negatively charged p-SWNT25, the shell thickness of the polymerized CTVB/NaSS monolayer and the SWNT diameter are 2.0 nm and 1 nm, respectively.

monolayers was considered. Therefore, two kinds of lipids, dioleoyltrimethylammoniumpropane (DOTAP) and dioleoylphosphatidylethanolamine (DOPE) (which are univalent cationic lipids with zero spontaneous curvature and zwitterionic lipids with negative spontaneous curvature, respectively) were used. CLs with different surface charge densities and spontaneous curvatures (25 mg mL^{-1}) were prepared by extruding various mixtures of DOTAP and DOPE (Φ_{DOPE} = 0.33, 0.5, 0.67, 0.75, 0.8, and 0.85, where Φ_{DOPE} is the weight fraction: DOPE/(DOTAP + DOPE)) through 200 nm Nuclepore filters. As the fraction of DOPE in CL increases, the surface charge density and spontaneous curvature of the lipid monolayer are simultaneously controlled, which may induce a topological phase transition of the complex as observed in the DNA–DOTAP/DOPE complex.[23] A conceptual idea of the interaction control of a p-SWNT25–CL complex is shown in Fig. 1. The p-SWNT25 and CLs with various Φ_{DOPE} were mixed in water under different CL/p-SWNT25 mass ratios (L/S), maintaining a total p-SWNT25 and CL concentration at 1.2 wt%. Dynamic light scattering (DLS) and zeta potential measurements showed that the p-SWNT25–CL mixtures formed large aggregates near the isoelectric points where the sign of the zeta potential was inversed (ESI†). As the Φ_{DOPE} is increased, the L/S mass ratio at the isoelectric points increases from 0.6 to 1.7 (Fig. 2a), since the positive surface charge density of the CL decreases with Φ_{DOPE}.

The self-assembly of p-SWNT25–CL complexes, which is driven by the release of bound counterions as p-SWNT25s and CLs compensate each other electrostatically,[46–49] most strongly occurred at their isoelectric points. Therefore, the structural characterization of p-SWNT25–CL complexes was performed at their isoelectric points. The structures of p-SWNT25–CL complexes for different Φ_{DOPE} were characterized by the small angle X-ray scattering (SAXS) measurements (which were performed at 25 °C using the 4C1 beamline at the Pohang Accelerator Laboratory, Korea). The p-SWNT25–CL complexes were equilibrated for one day at room temperature before SAXS measurements. All SAXS intensities of p-SWNT25–CL complexes at their isoelectric points show very sharp peaks, which indicate the formation of a highly ordered structure of p-SWNT25–CL complexes (Fig. 2b). It should be noted that as the Φ_{DOPE} is increased from 0.33 to 0.85, the scattering patterns of the complexes start to change at Φ_{DOPE} = 0.75, and are entirely changed at Φ_{DOPE} = 0.8, indicating a topological phase transition of the p-SWNT25–CL complexes near Φ_{DOPE} = 0.75.

The scattering peaks of the p-SWNT25–CL complexes with Φ_{DOPE} = 0.33, 0.5, and 0.67 at their isoelectric points can be indexed using two different sets of the ordered structures. Four peaks around q = 0.6 nm^{-1}, 1.2 nm^{-1}, 1.8 nm^{-1}, and 2.4 nm^{-1} (indicated by black arrows in Fig. 2b) can be indexed with (001), (002), (003), and (004) Bragg reflections of a multilamellar structure with repeat distances (d_{lam}) of 10.3 nm, 10.5 nm, and 10.7 nm for Φ_{DOPE} = 0.33, 0.5, and 0.67 (Fig. 2c),[50] respectively. On the other hand, the other 2 peaks around q = 1.27 nm^{-1} and 1.52 nm^{-1} (indicated by red arrows in Fig. 2b) can be indexed with (1,1) and (1,3) Bragg reflections of the centered rectangular columnar structure where the scattering peaks occur at $q_{hk} = 2\pi\sqrt{(h/a)^2 + (k/b)^2}$ (a and b are two-dimensional lattice parameters). Here, the lattice parameter b is set to be $2d_{lam}$

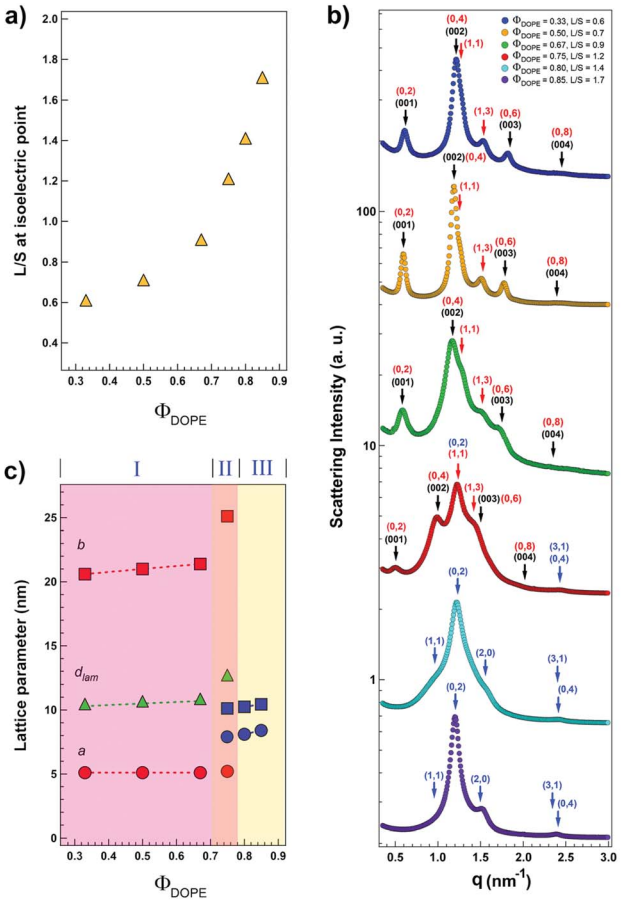

Fig. 2 (a) L/S mass ratio and (b) SAXS intensities of p-SWNT25–CL complexes at their isoelectric points. (c) Lattice parameters obtained from SAXS analyses of the complexes. An intercalated centered rectangular columnar superlattice of SWNTs (region I), a mixed phase (region II), and an inverted centered rectangular columnar superstructure (region III) are distinguished with colors.

(resulting in 20.6 nm, 21.0 nm, and 21.4 nm for Φ_{DOPE} = 0.33, 0.5, and 0.67, respectively) and the lattice parameter a is estimated to be a constant of 5.1 nm (ref. 51) which is close to the diameter of p-SWNT25 (Fig. 2c). The (0,2), (0,4), (0,6), and (0,8) indices of the centered rectangular structure are then completely overlapped with the (001), (002), (003), and (004) peaks of the multilamellar structure (Fig. 2b), respectively. The systematic absence of (h,k) peaks with $h + k = 2n + 1$ such as (0,3), (0,5), (1,2), (1,4), (0,7), and (1,6) in the accessible q range for this SAXS experiment further supports the centered symmetry of the lattice.[52] Considering the lipid bilayer thickness (*ca.* 4 nm) (ref. 53) and the lamellar repeat distance (*ca.* 10.5 nm), the water gap thickness of the multilamellar structure of the complex is *ca.* 6.5 nm, which is sufficient to accommodate one monolayer of p-SWNT25. All the results, including the fact that the lattice parameter b is equal to $2d_{lam}$, indicate that the p-SWNT25–CL complexes with Φ_{DOPE} = 0.33, 0.5, and 0.67 form an intercalated lamellar structure (in which the lipid bilayer and the p-SWNT25 monolayer alternate) with a centered rectangular symmetry of p-SWNT25 arrays (Fig. 3a). Similar structures were observed in the DNA–calcium–DPPC complex[54] and the DNA–DMPC/DMTAP complex.[55] The interlayer interaction to form the

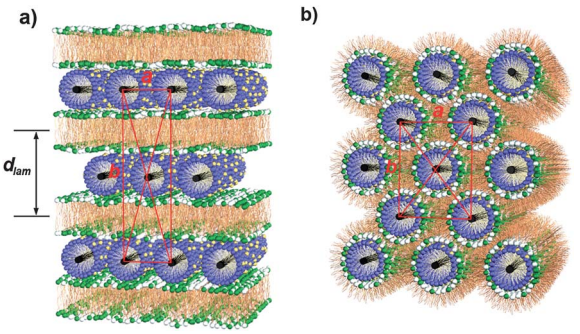

Fig. 3 (a) Intercalated lamellar structure with a centered rectangular columnar superlattice of p-SWNT25s. (b) Inverted centered rectangular columnar packing with p-SWNT25s at their centers. The green and white colors indicate DOTAP and DOPE, respectively.

intercalated lamellar structure with a centered rectangular symmetry of p-SWNT25s can be attributed to the synergetic effects of local elastic bending deformation of the lipid membrane and electrostatic repulsion across the membrane, which may arise from the local demixing of the cationic DOTAP and neutral DOPE lipid around the negatively charged p-SWNT25.[55] It should be noted that while the centered rectangular phase of the DNA–DMPC/DMTAP complex is formed only when lipids are in a gel phase, that of the p-SWNT25–CL complex is formed when lipids are in a fluidic phase. It should be also noted that, in the DNA–DOTAP/DOPE complex,[23] the centered rectangular symmetry of DNA distribution was not observed even though a one-dimensional lattice of DNAs intercalated in a lamellar structure was formed. These differences may be attributed to the high rigidity and straightness of p-SWNT25. The domain size of the complex with $\Phi_{DOPE} = 0.5$, which is estimated from the full width at half-maximum of (1,3) reflection using the Scherrer equation, is *ca.* 100 nm.

In the SAXS intensity of the p-SWNT25–CL complex with $\Phi_{DOPE} = 0.8$ and 0.85 (at which the spontaneous curvature of the lipid monolayer becomes more negative), the multilamellar peaks completely disappeared and a new set of peaks appeared (indicated by blue arrows in Fig. 2b), which indicates a topological phase transition. The new scattering peaks can be indexed with (1,1), (0,2), (2,0), (3,1) and (0,4) Bragg reflections of a centered rectangular columnar packing, with systematically missing (h,k) peaks with $h + k = 2n + 1$. The lattice parameters a and b for $\Phi_{DOPE} = 0.8$ and 0.85 are $a = 8.1$ nm and 8.4 nm and $b = 10.25$ nm and 10.45 nm, respectively (Fig. 2c). The absence of lamellar peaks and the enhanced negative spontaneous curvature of the lipid monolayer at high Φ_{DOPE} strongly support the transition from the intercalated lamellar structure (with a centered rectangular symmetry of p-SWNT25 array) into an inverted centered rectangular columnar packing with p-SWNT25 at the centers of columns (Fig. 3b). This is in contrast to the DNA–DOTAP/DOPE complex,[23] where a phase transition from the intercalated lamellar structure to an inverted hexagonal structure was observed as the fraction of DOPE was increased. The peak intensity of (1,1) reflection is fairly low or missing because the form factor of the p-SWNT25–CL complex with $\Phi_{DOPE} = 0.8$ and 0.85 along the $\vec{q}_{11}$ direction has a sharp dip near the (1,1) reflection position. The domain size of the complex at $\Phi_{DOPE} = 0.85$, which is estimated from the full width at half-maximum of (0,2) reflection using the Scherrer equation, is *ca.* 90 nm.

The topological transition from the intercalated lamellar to the inverted hexagonal columnar phase has been explained in terms of the interplay between electrostatic interaction and membrane elastic interaction in the complex.[23] While the attractive electrostatic interactions between the negatively charged cylindrical particles and the cationic lipids are expected to favor an inverted hexagonal phase, it is opposed by the Helfrich elastic energy cost of forming a cylindrical monolayer membrane around the cylindrical particles:

$$F/A = 0.5\kappa(1/R - 1/R_0)^2$$

where κ is the lipid monolayer rigidity, R is the radius of curvature, and R_0 is the spontaneous radius of curvature. It has been shown that either decreasing the bending rigidity or the difference between the curvature and the spontaneous curvature of the lipid membrane can reduce the elastic bending energy cost to form a cylindrical lipid monolayer around the cylindrical particles. In our experiments, the bending energy cost was mainly controlled by changing the spontaneous curvature of the lipid membrane. While DOTAP has a zero spontaneous curvature ($1/R_0^{DOTAP} = 0$) that favors a flat membrane, the DOPE has a negative spontaneous curvature ($1/R_0^{DOPE} < 0$) that favors an inverted curved membrane. Therefore, as Φ_{DOPE} increases, the elastic energy cost to form an inverted cylindrical monolayer around the p-SWNT25 is reduced, making the electrostatic interaction more dominant. Therefore, it is expected that the elastic bending energy cost decreases sufficiently to form a cylindrical lipid monolayer around the p-SWNT25 at a certain critical Φ_{DOPE} (near $\Phi_{DOPE} = 0.75$, Fig. 2b), inducing a topological phase transition.

Considering that p-SWNT25s are cylindrical particles, it is unexpected that the p-SWNT25–CL complex adopts an inverted centered rectangular columnar packing rather than an inverted hexagonal columnar packing. This may be understood in terms of the correlated effects of demixing and the different spontaneous curvatures of DOTAP and DOPE. The initial adsorption of p-SWNT25 on the membrane may induce demixing of DOTAP and DOPE due to electrostatic interaction between cationic lipids (DOTAP) and anionic cylinders (p-SWNT25). While DOTAP with a zero spontaneous curvature prefers a flat membrane (along the a axis), DOPE with a negative spontaneous curvature ($-1/2.83$ nm^{-1}) (ref. 56) prefers an inverted curved membrane (along the b axis), which may result in the anisotropic pocket surrounding the p-SWNT25 (Fig. 3b). Furthermore, since the thicknesses of the lipid headgroups are different (4.5 Å for DOTAP[57] and 8 Å for DOPE[58]) while their chain lengths are the same, the thicknesses of the lipid headgroup region along the a and b axes may have a disparity, further increasing the anisotropy of the pocket surrounding the p-SWNT25. This anisotropy may have induced the centered rectangular packing of the p-SWNT25–CL complex rather than hexagonal packing. It is worth noting that, in a previous study by Huang *et al.*,[59] it was reported that the DOPE/DOPC mixture shows a distorted hexagonal phase due to lipid demixing (with a higher DOPE/DOPC ratio at a higher curvature region).

The scattering pattern of the p-SWNT25–CL complexes at $\Phi_{DOPE} = 0.75$ (where the scattering pattern started to change) indicates that it is a mixed phase of the intercalated lamellar structure with centered rectangular packing of p-SWNT25 and the inverted centered rectangular columnar packing with p-SWNT25 at the centers of columns. The peak indexing for different structures are distinguished with different colors (black for multilamellar, red for intercalated centered rectangular, and blue for inverted centered rectangular packing). The lattice parameters for each superstructure determined from SAXS intensities are presented in Fig. 2c.

The L/S ratios are calculated from the p-SWNT25–CL superstructures (determined from the SAXS measurements), resulting in L/S = 0.52, 0.54, 0.55, 1.13, and 1.26 for $\Phi_{DOPE} = 0.33$, 0.5, 0.67, 0.8, and 0.85, respectively. In this calculation, it was assumed that there were no defects in the superstructures. The calculated L/S ratios are rather smaller than the initial composition ratios of samples (L/S = 0.6, 0.7, 0.9, 1.4, and 1.7 for $\Phi_{DOPE} = 0.33$, 0.5, 0.67, 0.8, and 0.85, respectively), although the overall trends of the two L/S ratios are consistent with each other. The difference in the L/S ratios may be attributed to the possible elastic membrane deformation induced by p-SWNT25 (ref. 51) or the defects of superstructures due to the length polydispersity of p-SWNT25, which could not be considered in the calculation.

Conclusions

Negatively charged SWNTs and mixed cationic liposome complexes at the isoelectric point exhibit two kinds of superlattices of SWNTs depending on the spontaneous curvature and surface charge density of the lipid bilayer which are controlled by the mixing ratio of DOPE and DOTAP. When the mixing ratio of DOPE and DOTAP is low, the p-SWNT25–CL complex forms a centered rectangular superlattice of SWNTs intercalated in a multilamellar structure. As the lipid mixing ratio increases, making the spontaneous curvature and surface charge density of lipid bilayer more negative and smaller, respectively, the p-SWNT25–CL complex transforms into an inverted centered rectangular columnar packing with SWNTs at the centers of columns. The results of this study may provide a new route to fabricate highly ordered superlattices of SWNTs with new or enhanced functionalities, utilizing biomolecular self-assembling behavior. This may also provide a new insight into the interactions of functionalized SWNTs in lipid membranes, which are essential for the biological or biomedical applications of SWNTs such as drug delivery.

Acknowledgements

This work was supported by National Research Foundation grants funded by the Ministry of Education, Science and Technology of the Korean government (no. 2012-0000177 and no. 2011-0031931) and a grant from the Construction Technology Innovation Program funded by the Ministry of Land, Transportation and Maritime Affairs of the Korean government.

Notes and references

1 S. J. Tans, A. R. M. Verschueren and C. Dekker, *Nature*, 1998, **393**, 49.
2 C. Zhou, J. Kong, E. Yenilmez and H. Dai, *Science*, 2000, **290**, 1552.
3 K. H. An, W. S. Kim, Y. S. Park, Y. C. Choi, S. M. Lee, D. C. Chung, D. J. Bae, S. C. Lim and Y. H. Lee, *Adv. Mater.*, 2001, **13**, 497.
4 P. M. Ajayan, L. S. Schadler, C. Giannaris and A. Rubio, *Adv. Mater.*, 2000, **12**, 750.
5 V. P. Veedu, A. Cao, X. Li, K. Ma, C. Soldano, S. Kar, P. M. Ajayan and M. N. Ghasemi-Nejhad, *Nat. Mater.*, 2006, **5**, 457.
6 R. Saito, G. Dresselhaus and M. S. Dresselhaus, *Physical Properties of Carbon Nanotubes*, Imperial College Press, London, U.K., 1998.
7 M. S. Dresselhaus, G. Dresselhaus and P. Avouris, *Carbon Nanotubes Synthesis, Structure, Properties, and Applications*, Springer-Verlag, New York, 2003.
8 P. Harris, *Carbon Nanotubes and Related Structures*, Cambridge University Press, Cambridge, U. K., 1999.
9 R. Yang, J. Jin, Y. Chen, N. Shao, H. Kang, Z. Xiao, Z. Tang, Y. Wu, Z. Zhu and W. Tan, *J. Am. Chem. Soc.*, 2008, **130**, 8351.
10 X. Chen, U. C. Tam, J. L. Czlapinski, G. S. Lee, D. Rabuka, A. Zettl and C. R. Bertozzi, *J. Am. Chem. Soc.*, 2006, **128**, 6292.
11 C. H. Villa, M. R. McDevitt, F. E. Escorcia, D. A. Rey, M. Bergkvist, C. A. Batt and D. A. Scheinberg, *Nano Lett.*, 2008, **8**, 4221.
12 B. Kang, D. Yu, Y. Dai, S. Chang, D. Chen and Y. Ding, *Small*, 2009, **5**, 1292.
13 L. N. Cella, W. Chen, N. V. Myung and A. Mulchandani, *J. Am. Chem. Soc.*, 2010, **132**, 5024.
14 L. Meng, J. Jin, G. Yang, T. Lu, H. Zhang and C. Cai, *Anal. Chem.*, 2009, **81**, 7271.
15 R. J. Chen, S. Bangsaruntip, K. A. Drouvalakis, N. W. S. Kam, M. Shim, Y. Li, W. Kim, P. J. Utz and H. Dai, *Proc. Natl. Acad. Sci. U. S. A.*, 2003, **100**, 4984.
16 T. Fujigaya, T. Morimoto and N. Nakashima, *Soft Matter*, 2011, **7**, 2647.
17 R. Sharma, C. Y. Lee, J. H. Choi, K. Chen and M. S. Strano, *Nano Lett.*, 2007, **7**, 2693.
18 S. G. Rao, L. Huang, W. Setyawan and S. Hong, *Nature*, 2003, **425**, 36.
19 N. Akima, Y. Iwasa, S. Brown, A. M. Barbour, J. Cao, J. L. Musfeldt, H. Matsui, N. Toyota, M. Shiraishi, H. Shimoda and O. Zhou, *Adv. Mater.*, 2006, **18**, 1166.
20 H. Ko and V. V. Tsukruk, *Nano Lett.*, 2006, **6**, 1443.
21 P. V. Kamat, K. G. Thomas, S. Barazzouk, G. Girishkumar, K. Vinodgopal and D. Meisel, *J. Am. Chem. Soc.*, 2004, **126**, 10757.
22 C. Doe, H.-S. Jang, T.-H. Kim, S. R. Kline and S.-M. Choi, *J. Am. Chem. Soc.*, 2009, **131**, 16568.
23 I. Koltover, T. Salditt, J. O. Rädler and C. R. Safinya, *Science*, 1998, **281**, 78.
24 J. O. Rädler, I. Koltover, T. Salditt and C. R. Safinya, *Science*, 1997, **275**, 810.
25 K. K. Ewert, H. M. Evans, A. Zidovska, N. F. Bouxsein, A. Ahmad and C. R. Safinya, *J. Am. Chem. Soc.*, 2006, **128**, 3998.
26 H. Liang, D. Harries and G. C. L. Wong, *Proc. Natl. Acad. Sci. U. S. A.*, 2005, **102**, 11173.
27 N. F. Bouxsein, C. Leal, C. S. McAllister, K. K. Ewert, Y. Li, C. E. Samuel and C. R. Safinya, *J. Am. Chem. Soc.*, 2011, **133**, 7585.
28 Z. Liu, X. Sun, N. Nakayama and H. Dai, *ACS Nano*, 2007, **1**, 50.
29 A. Bianco, K. Kostarelos and M. Prato, *Curr. Opin. Chem. Biol.*, 2005, **9**, 674.
30 Z. Liu, K. Chen, C. Davis, S. Sherlock, Q. Cao, X. Chen and H. Dai, *Cancer Res.*, 2008, **68**, 6652.
31 C. H. Villa, M. R. McDevitt, F. E. Escorcia, D. A. Rey, M. Bergkvist, C. A. Batt and D. A. Scheinberg, *Nano Lett.*, 2008, **8**, 4221.
32 N. W. S. Kam, M. O'Connell, J. A. Wisdom and H. Dai, *Proc. Natl. Acad. Sci. U. S. A.*, 2005, **102**, 11600.
33 A. A. Bhirde, W. Patel, J. Gavard, G. Zhang, A. A. Sousa, A. Masedunskas, R. D. Leapman, R. Weiger, J. S. Gutkind and J. F. Rusling, *ACS Nano*, 2009, **3**, 307.
34 L. Meng, X. Zhang, Q. Lu, Z. Fei and P. J. Dyson, *Biomaterials*, 2012, **33**, 1689.
35 V. V. Chaban and O. V. Prezhdo, *ACS Nano*, 2011, **5**, 5647.
36 T.-H. Kim, S.-M. Choi and S. R. Kline, *Langmuir*, 2006, **22**, 2844.
37 T.-H. Kim, C. Doe, S. R. Kline and S.-M. Choi, *Adv. Mater.*, 2007, **19**, 929.
38 T.-H. Kim, C. Doe, S. R. Kline and S.-M. Choi, *Macromolecules*, 2008, **41**, 3261.
39 M. J. O'Connell, S. M. Bachilo, C. B. Huffman, V. C. Moore, M. S. Strano, E. H. Haroz, K. L. Rialon, P. J. Boul, W. H. Noon, C. Kittrell, J. Ma, R. H. Hauge, R. B. Weisman and R. E. Smalley, *Science*, 2002, **297**, 593.

40 A. M. Rao, E. Richter, S. Bandow, B. Chase, P. C. Eklund, K. A. Williams, S. Fang, K. R. Subbaswamy, M. Menon, A. Thess, R. E. Smalley, G. Dresselhaus and M. S. Dresselhaus, *Science*, 1997, **275**, 187.
41 X. Zhang, T. Liu, T. V. Sreekumar, S. Kumar, V. C. Moore, R. H. Hauge and R. E. Smalley, *Nano Lett.*, 2003, **3**, 1285.
42 V. C. Moore, M. S. Strano, E. H. Haroz, R. H. Hauge and R. E. Smalley, *Nano Lett.*, 2003, **3**, 1379.
43 A. G. Ryabenko, T. V. Dorofeeva and G. I. Zvereva, *Carbon*, 2004, **42**, 1523.
44 A. Di Crescezo, D. Demurtas, A. Renzetti, G. Siani, P. De Maria, M. Meneghetti, M. Prato and A. Fontana, *Soft Matter*, 2009, **5**, 62.
45 When all the counterions are copolymerized on the surface of p-SWNT25s, the surface charge density is estimated to be $1e^{-}/264\ \text{Å}^{-2}$.
46 L. Yang, H. Liang, T. E. Angelini, J. Butler, R. Coridan, J. X. Tang and G. C. L. Wong, *Nat. Mater.*, 2004, **3**, 615.
47 I. Koltover, K. Wagner and C. R. Safinya, *Proc. Natl. Acad. Sci. U. S. A.*, 2000, **97**, 14046.
48 I. Koltover, T. Salditt and C. R. Safinya, *Biophys. J.*, 1999, **77**, 915–924.
49 T.-H. Kim, S.-H. Kang, C. Doe, J. Yu, J.-B. Sim, J. Kim, S. R. Kline and S.-M. Choi, *J. Am. Chem. Soc.*, 2009, **131**, 7456.
50 Since the lipid bilayer thickness of pure DOPE (4.42 nm) (ref. 60) is larger than that of DOTAP (3.72 nm) (ref. 57), the bilayer thickness of the mixed lipid increases with Φ_{DOPE}, resulting in the slight increase of the lamellar repeat distance.
51 Considering that the positive surface charge density of a lipid bilayer decreases with increasing the Φ_{DOPE}, it is rather unexpected that the lattice parameter a (which is the center-to-center distance between neighboring p-SWNT25s) does not increase with the Φ_{DOPE}. The origin is not clear but it may be related to elastic membrane deformation induced by p-SWNT25.
52 T. Hahn, *International Tables for Crystallography Vol A: Space Group Symmetry*, Kluwer Academic Publisher, London, U.K., 3rd edn, 1992.
53 The thicknesses of lipid bilayer ($\Phi_{\text{DOPE}} = 0.33, 0.5, 0.67$) were estimated by the weighted average of each pure lipid bilayer thickness (3.72 nm for DOTAP (ref. 57) and 4.42 nm for DOPE (ref. 60)), resulting in *ca.* 4 nm.
54 J. J. McManus, J. O. Rädler and K. A. Dawson, *J. Am. Chem. Soc.*, 2004, **126**, 15966.
55 F. Artzner, R. Zantl, G. Rapp and J. O. Rädler, *Phys. Rev. Lett.*, 1998, **81**, 5015.
56 R. M. Epand, N. Fuller and R. P. Rand, *Biophys. J.*, 1996, **71**, 1806.
57 J. O. Rädler, I. Koltover, A. Jamieson, T. Salditt and C. R. Safinya, *Langmuir*, 1998, **14**, 4272.
58 M. Rappolt, A. Hickel, F. Bringezu and K. Lohner, *Biophys. J.*, 2003, **84**, 3111.
59 L. Ding, T. M. Weiss, G. Fragneto, W. Liu, L. Yang and H. W. Huang, *Langmuir*, 2005, **21**, 203.
60 O. Francescangeli, M. Pisani, V. Stanić, P. Bruni and T. M. Weiss, *Europhys. Lett.*, 2004, **67**, 669.

